PCCP

Accepted Manuscript

ROYAL SOCIETY OF CHEMISTRY

www.rsc.org/pccp

ARTICLE TYPE www. rsc.org/xxxxxx | XXXXXXXX

Solid state effects on the electronic structure of H_2OEP †

M. Marsili,*[a,b] P. Umari,[a,c] G. Di Santo,[d] M. Caputo,[d] M. Panighel,[d,e] A. Goldoni,[d] M. Kumar,[f] and M. Pedio [f]

Received Xth XXXXXXXXXX 20XX, Accepted Xth XXXXXXXXX 20XX
First published on the web Xth XXXXXXXXXX 200X
DOI: 10.1039/b000000x

We present the results of a joint experimental and theoretical investigation concerning the effect of crystal packing on the electronic properties of the H_2OEP molecule. Thin films, deposited in ultra high vacuum on metal surfaces, are investigated combining valence band photoemission, inverse photoemission, and x-ray absorption spectroscopies. The spectra of the films are compared, when possible, with those of measured in gas phase. Once many-body effects are included in the calculations through the GW method, the electronic structure of the film and of the gas phase are accurately reproduced for both valence and conduction states. Upon going from an isolated molecule to the film phase, the electronic gap shrinks significantly and the lowest unoccupied molecular orbital (LUMO) and the LUMO+1 degeneracy is removed. The calculations show that the reduction of the transport gap in the film is entirely addressable to the enhancement of the electronic screening.

1 Introduction

Porphyrins belong to a class of molecules that has been intensively studied for its importance in biology and natural processes[1]. From the technological point of view, there are possible applications in a variety of fields such as catalysis, optoelectronics and photovoltaics[2–4]. The applicative potentiality of this kind of molecules and their involvement in fundamental biological processes are due to the great diversity of functionalities that can be achieved by changing their building blocks, i.e. using different functional groups and/or metal centers[5]. Interestingly, in this way, it is possible, not only to control the properties of a single molecule, but also to control how the molecules assemble and pack, thus tailoring, for instance, the crystal structure or the size of the void space between aggregates, and providing a further path for specific functionalizations[6,7]. In view of the application of this kind of molecules in their solid state form, we study the effect of crystal packing on the electronic structure of H_2OEP, one of the simplest molecules of this class. The choice of this specific molecule among all the possible other porphyrins is based on the fact that it presents a single crystalline phase, thus favoring the comparison between theoretical prediction and experimental results.

A direct and accurate determination of the electronic levels of molecular solids and films is extremely desirable for a variety of applications, as in optoelectronics, catalytic or magnetic systems. Combined valence-band photoemission (PES) and inverse photoemission (IPS) spectroscopies studies allow the direct determination of the relevant transport levels[8,9]. This kind of studies has been applied to the determination of the electronic structures of several organic films made of phtalocyanines[8,10–13], perylene derivatives (PTCDA)[8,13–15], Alq3 (aluminum tris-8-hydroxyquinoline)[12,13], fullerenes[16], bithiophene[17], and α-NPD (N,N'-diphenyl-N,N'-bis(1-naphthyl)-1, 1'-biphenyl-4,4" diamine)[12] films. A few PES-IPS studies on porphyrin films are reported[18–21]; in these works the interaction of the molecules with the different substrates they were grown on was studied in detail. However, the effect of crystal packing was not analyzed, and there are no studies, to the best of our knowledge, where both the valence and conduction bands of porphyrin films have been theoretically addressed, with the inclusion of many-body effects, in comparison with the experimental data.

The electronic structure of the H_2OEP molecule has been extensively studied in gas phase[22]. For the isolated molecule, the experimental and the theoretical density of occupied states was determined[23]. Therefore we employ direct and inverse photoemission spectroscopy as well as near-edge x-ray absorption fine-structure (NEXAFS) spectroscopy to probe directly the density of occupied and unoccupied electronic levels of H_2OEP thin films grown on metal substrates. The

† Electronic Supplementary Information (ESI) available: DFT and GW band structures.

[a] *Dipartimento di Fisica e Astronomia, Universitá di Padova, via Marzolo 8, Padova 35131, Italy. Fax: +39 049 8277102; Tel: +39 049 8277174; E-mail: margherita.marsili@nano.cnr.it*
[b] *S3, Istituto Nanoscienze-CNR, Via Campi 213/A, 41125 Modena, Italy*
[c] *IOM-CNR, Theory@Elettra group, Trieste, Italy*
[d] *Elettra - Sincrotrone Trieste, s.s. 14 km 163.5 in Area Science Park, Basovizza (Trieste) 34149, Italy*
[e] *Department of Physics, University of Trieste, via Valerio 2, Trieste 34100, Italy*
[f] *IOM-CNR, TASC Area Science Park Buil. MM, S.S. 14, Km 163.5, Basovizza (Trieste) 34149, Italy*

experimental spectra are then analyzed and compared with the results of state-of-the-art ab-initio electronic structure calculations based on many-body perturbation theory (MBPT) through the GW method. We have found that the GW method can accurately reproduce the experimental spectra both for the gas and the solid phases. This allows us to trace the origin of the band gap reduction observed for thin films.

The paper is organized as follows: in Sect. 2 the experimental and theoretical methods are addressed; in Sect. 3 we present and discuss the results concerning the geometry and the electronic structure of H_2OEP, comparing gas and solid state phases; in Sect. 4 the conclusions are drawn.

2 Methods

2.1 Experimental

All the experiments were performed in ultra-high vacuum (UHV) experimental chambers at a base pressure better than of 10^{-10} mbar. Highly purified (99%) commercial H_2OEP was used and sublimated at 520 K using a home made, resistively heated, Ta evaporator. The H_2OEP multilayer films were deposited in UHV on clean Ag(111) substrate for thicknesses from 1 to 40 nm. The H_2OEP films were characterized ex situ by X-ray diffraction (XRD), which confirmed the triclinic structure of the film in good agreement with reported X-ray studies[24,25].

The measurements relative to H_2OEP molecules in gas phase were carried out at the gas phase beamline at Elettra using a 150 mm hemispherical electron energy analyzer. The valence band spectrum of H_2OEP was collected with an incident photon energy of 120 eV and an overall energy resolution (photons+analyzer) of 0.20 eV. The energy scale was calibrated using, by reference, the water spectrum. NEXAFS spectra at the N 1s threshold were collected in partial electron yield mode and the energy scales were calibrated by introducing N_2 in the chamber, collecting a N_2 molecule spectrum, and using the N_2 reference value to align the energies.

The valence band photoemission data for a multilayer film (evaporated on clean Ag(111) substrate) were collected at the Micro Nano Carbon laboratory by means of a VG 150 hemispherical electron energy analyzer in normal emission using He I radiation (21.22 eV) with an energy resolution of 0.1 eV. The binding energies of the photoemission spectra were calibrated using the Fermi level of Ag(111). The NEXAFS spectra at the N 1s thresholds for the multilayer film were collected at the BACH beamline and already reported in ref.[26].

The angle resolved inverse photoemission (IPS) measurements at normal incidence were performed at the SIPE-TASC laboratory using a home made Erdman-Zipf electron gun. The electron beam divergence was better than 3°. Photons emitted from the sample surface were collected by a homemade Geiger-Mueller type detector with a He-I_2 gas mixture and a SrF_2 entrance window filtering photons at a hν= 9.5 eV energy. The experimental resolution was $\leq$ 350 meV, as measured by the Fermi level onset of a clean Ta foil which was frequently interchanged with the sample. In order to prevent degradation of the molecular film, the beam current density was limited to 8×10^{-7} A/cm^2. No charging was detected during acquisition. Damage produced by the electrons beam has been found after 1 hour of IPS acquisition. To further reduce the degradation of the molecular film during measurements, the spectra were acquired onto different samples, prepared in the same way, and at various sample locations, changed after about 20 minutes of acquisition. The single scans were numerically summed subsequently. The IPS spectra shown in this paper are taken on a H_2OEP film whose thickness was about 5 nm, the value beyond which no further band shift was detectable.

2.2 Theoretical

The accurate first-principle determination of the electronic density of states (DOS) of the H_2OEP molecule and film is achieved in a two step procedure: (i) the ground state equilibrium geometry is obtained within density-functional theory (DFT); (ii) the single particle excitation energies of the system are addressed within MBPT employing the GW method.

In the following, we will provide a brief overview of the latter method which is extensively reviewed in Ref.[27] and Ref.[28].

The GW method Within MBPT, it can be shown that the poles of the single-particle Green's function are found at frequencies that correspond to the charged excitation energies of the electronic system. The GW method allows for an accurate determination of the poles of the single particle Green's function, thus providing a reliable estimation of the electronic DOS as probed by PE.

In the frequency domain, the single particle Green's function, can be expressed as:

$$G(\mathbf{r},\mathbf{r}';\omega) = \sum_{nk} \frac{\psi_{nk}(\mathbf{r},\omega)\tilde{\psi}^*_{nk}(\mathbf{r}',\omega)}{\omega - \varepsilon_{nk}(\omega)} \tag{1}$$

where $\varepsilon_{nk}(\omega)$, $\psi_{nk}(\mathbf{r},\omega)$ are solution of the equation:

$$\begin{aligned}&\left[-\frac{\nabla^2}{2} + v_{ext}(\mathbf{r}) + v_H(\mathbf{r})\right]\psi_{nk}(\mathbf{r},\omega) + \\ &+ \int d\mathbf{r}'\Sigma(\mathbf{r},\mathbf{r}';\omega)\psi_{nk}(\mathbf{r}',\omega) = \varepsilon_{nk}(\omega)\psi_{nk}(\mathbf{r},\omega)\end{aligned} \tag{2}$$

Here v_{ext} is the external ionic potential, v_H is the Hartree potential, Σ is the electronic self-energy, and n and k are the band and k-point indices respectively. All quantities are expressed in atomic units (a.u.). The poles of the Green's function are

found at the quasiparticle energies ω_{QP}, that obey the relation $\omega_{nk}^{QP} = \varepsilon_{nk}(\omega_{nk}^{QP})$.

In order to solve Eq. 2, and to find the quasiparticle energies, an expression for Σ must be provided. A good approximation, that can be derived within the MBPT framework, is the so called GW approximation, where the electronic self-energy is given, in the time domain, by the simple product of the single particle Green's function G and the screened Coulomb interaction W. Namely $\Sigma(1,2) = iG(1,2)W(1^+,2)$, where $1^+ = (\mathbf{r}_1, t_1 + \eta)$ and η is an infinitesimal positive number.

The screened Coulomb interaction can be expressed in terms of the reducible polarizability P as $W(1,2) = v(1,2) + \int d3d4 v(1,3)P(3,4)v(4,2) = v(1,2) + W_c(1,2)$, where $v(1,2)$ is the bare Coulomb potential. The last relation defines W_c, which is the frequency dependent part of the screened interaction. Thus Σ can be expressed as the sum of an exchange term, $\Sigma_x(1,2) = iG(1,2)v(1^+,2)$, and of a correlation term, $\Sigma_c(1,2) = iG(1,2)W_c(1^+,2)$. By neglecting Σ_c ,the Hartree-Fock picture is recovered.

Besides using an approximate form for Σ, in actual calculations further approximations are carried out. In this work we employ the so called G_0W_0 approximation, where the single particle Green's function, entering in the expression of Σ, is the non-interacting DFT Kohn Sham (KS) Green's function; the electronic screening is built, at the RPA level, employing KS energies and wavefunctions; and the $\psi_{nk}(\mathbf{r},\omega)$, in the quasiparticle equation 2, are approximated by the KS states.

The frequency dependence of the screening is fully taken into account in our calculations. In order to carry out this task, Σ_c is evaluated along the imaginary frequency axis and then analytically continued to the real axis[29,30] after fitting $\Sigma_c(i\omega)$ with a multipole function. Another possible approach is the so called contour deformation method[31,32]. Within this method the integrals along the real frequency axis are evaluated in terms of integrals over the imaginary axis plus a summation over poles; in this way the fitting procedure is avoided. The contour deformation method is very accurate but extremely demanding from a computational point of view. We employed it to compute the energy levels close to the highest occupied molecular orbital (HOMO)-LUMO levels, and to optimize the fit parameters of the analytic continuation method.

We compare the calculated DOS directly with experimental spectra neglecting matrix-element effects. Usually this approximation leads to a good agreement with experiments[23].

Computational details The DFT calculations were performed using the QUANTUM ESPRESSO package[33]. Norm-conserving pseudopotentials and the PBE[34] exchange-correlation functional were used throughout the calculations. The energy cutoff for the plane-wave expansion of the wavefunctions was set to 45 Ry. The Brillouin zone of the crystal was sampled at the Γ point.

For the crystal phase, the experimental lattice parameters were used[24], the relaxation of the atomic positions ended when all components of all forces were smaller than 1×10^{-4}a.u. The starting atomic coordinates within the crystal cell where obtained from the Ref.[24] and then the system was allowed to fully relax.

The GW calculations were performed using the GWL code within the QUANTUM ESPRESSO package[33]. In the isolated case the calculations were carried out using an orthorombic cell of $(25 \times 25 \times 12)^3$. In order to avoid spurious interaction between periodic replicas, we employed a 10 radius spherical cutoff for the Coulomb interaction. In both the isolated case and in the crystal phase, following the notation of Ref.[35], we employed an $E^* = 5$ Ry cutoff to build the optimal polarizability basis set, which we choose to be made of 2000 elements. This choice corresponds to a polarizability eigenvalue threshold of $q^* = 42$ Bohr$^3 = 8 \times 10^{-4}\Omega$ for the isolated case, and $q^* = 4.4$ Bohr$^3 = 9 \times 10^{-4}\Omega$ for the crystal phase calculations (here Ω is the unit cell volume of each calculation). The overall convergence for the determination of the levels close to the HOMO and LUMO is ~ 0.1 eV.

3 Results and discussion

Once organic molecules pack forming a molecular crystal, the geometry of each molecule becomes distorted with respect to the gas phase and, at the same time, the electronic properties of the system drastically change[36–41]. Such change may be an effect of the geometric distortion and/or due to modifications in the electronic screening, more effective in a 3D system. In the following section the results concerning the ground-state geometry and the electronic properties of the H_2OEP molecule and film are presented and discussed.

3.1 Geometry

In the H_2OEP molecule, eight ethyl groups are attached to the β carbon atoms of the porphine pyrrole rings[42], as shown in Fig. 1. In gas phase, the carbon skeleton of the molecule is essentially planar, the deviation of the calculated coordinates from the mean plane is less than 10^{-4} for the macrocycle-atoms .

H_2OEP crystallizes in a triclinic lattice with one molecule per unit cell. As our calculation scheme does not involve van der Waals corrections, we employed the experimental lattice structure parameters taken from Ref.[24], namely: $a = 9.791$, $b = 10.771$, $c = 7.483$, $\alpha = 97.43°$, $\beta = 106.85°$, $\gamma = 93.25°$.

As common for other porphyrins aggregates, within the crystal the H_2OEP molecules are arranged with parallel π systems, no relative rotation, and a finite center-to-center offset.

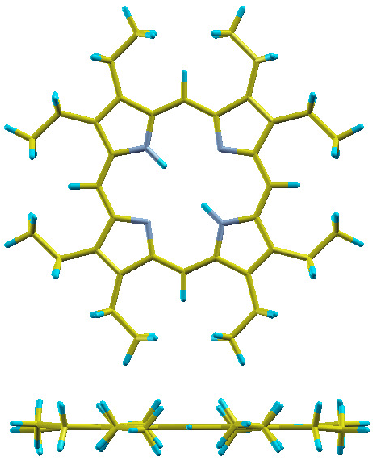

Figure 1 Equilibrium geometry of the isolated molecule. Carbon atoms in yellow, hydrogen atoms in cyan, nitrogen atoms in light blue. Top figure: top view; bottom figure: side view.

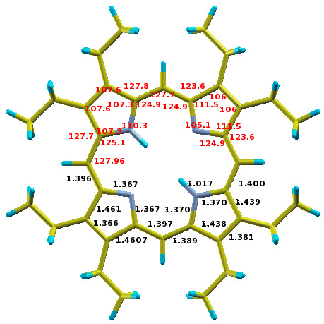

Figure 2 Geometry of the single H_2OEP molecule within the crystal.

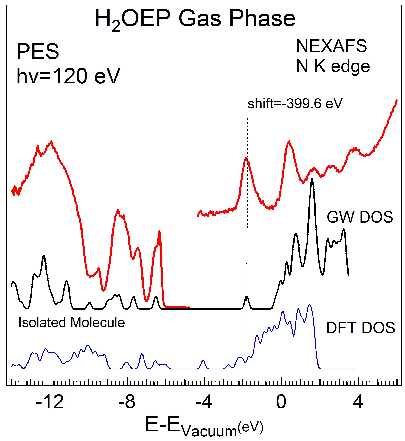

Figure 3 Density of occupied and unoccupied electronic states for the H_2OEP molecule in gas phase. Upper curves in red: experimental results from PES (occupied states) and NEXAFS (unoccupied states). Middle curve in black: computed GW DOS. Lower blue curve: computed DFT DOS. All energies are referred to the vacuum level.

The extent of such offset is determined by the interplay between van der Waals attraction and electrostatic repulsion[43]. At odds with the gas phase geometry, within the crystal, the ethyl groups of each molecule are oriented almost perpendicularly with respect to the average macrocycle plane. Two subsequent phenyl groups couples stick inward of the macrocycle plane, and the remaining subsequent two outwards. This is a typical geometry for the triclinic arrangement of this class of molecules[44].

In Fig. 2 the final geometry of the molecule in the triclinic phase is shown, together with the macrocycle bond-lengths (in red) and angles (in black). Once the angles and bonds that involve hydrogen atoms are neglected, because their position is determined with less accuracy by XRD, we obtain a mean relative deviation from the experimental geometry[24] of 0.38% concerning bond lengths and of 0.30% concerning angles.

In the crystalline form, the macrocycle is slightly ruffled, we find for the fully relaxed geometry a mean absolute displacement from the average plane of 0.026 , compatible with experimental results reported in Ref.[24] where a value of 0.021 ± 0.02 is found.

The shortest intermolecular distance,2.3 Å, is between a methylene hydrogen atom and an hydrogen atom bonded to a meso carbon belonging to molecules displaced by (011) (in primitive lattice units). In Ref.[24] a shortest intermolecular distance of 2.4 Å is reported, confirming the agreement between the experimental and theoretical geometry.

3.2 Electronic Structure

Isolated molecule The isolated molecule DOS, computed at the DFT and GW level, is shown in Fig. 3 together with the measured PES and NEXAFS. The first peak of the N K edge NEXAFS is aligned to to the computed GW LUMO level. The N K-edge NEXAFS spectrum for the transition N1s-LUMO, shows two peaks, labeled L_1 and L_2, due to initial state effects of the N 1s core level doublet excitation and related to the presence of two inequivalent N species in the molecule macrocycle[45].

The computed isolated molecule energy levels close to the gap are reported in Tab. 1. The ionization potential (IP) of the molecule in gas-phase is predicted to be 5.9 eV, close to the measured value of 6.3 eV, and to the previously computed value of 5.7 eV[23]. The discrepancy between the two calculations might be explained taking into account that the calcu-

Table 1 Computed HOMO-1, HOMO, LUMO, LUMO+1 energy levels for the isolated H_2OEP molecule. Energies are referred to the vacuum level E_{Vacuum}

Gas phase	HOMO-1 (eV)	HOMO (eV)	LUMO (eV)	LUMO+1 (eV)	GAP (eV)
DFT	-4.6	-4.4	-2.4	-2.4	2.0
GW	-5.9	-5.9	-1.2	-1.2	4.7
HF ($\Sigma_c = 0$)	-5.5	-5.8	0.9	1.0	6.7

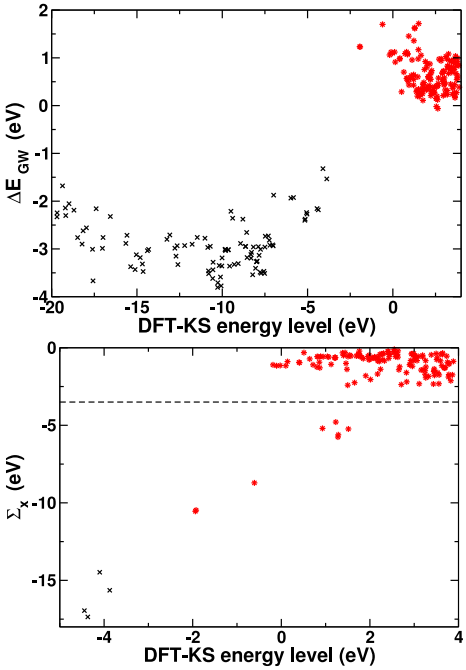

Figure 4 Top panel: GW corrections as a function of KS energy for the isolated H_2OEP molecule. Bottom panel: Σ_x as a function of KS energies. Black crosses refer to occupied energy levels, while red stars to unoccupied ones.

lation methods of Ref.[23] involved (truncated) summations on empty states, while here explicit summations of such a kind are exactly avoided.

At the DFT level, when many-body effects are neglected, the IP (4.4 eV) is strongly underestimated and the HOMO-LUMO gap is much smaller than in the GW calculation: the gap being 2.0 eV within DFT, while 4.7 eV within GW (see Tab. 1). In the previous GW calculation[23], a slightly smaller value of 4.4 eV was reported for the electronic gap, which is consistent with the difference found in the IPs values.

As the occupied part of the DOS was extensively analyzed in Ref.[23], here we focus on the unoccupied levels, which in the gas phase are experimentally probed by NEXAFS.

Once the GW DOS and the NEXAFS signal are aligned by setting the same energy for the LUMO, the two curves present

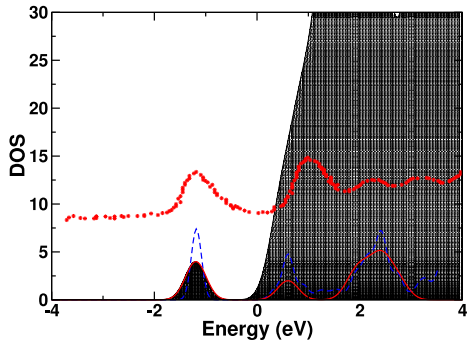

Figure 5 Comparison of computed GW DOS for the isolated molecule, and gas-phase NEXAFS. Black shaded area: full GW-DOS of the H_2OEP isolated molecule from Fig. 3; red line: GW DOS obtained taking into only the states for which $|<\Sigma_x>| > 3.5$ eV; blue-dashed line: projected DOS onto the macrocycle carbon and nitrogen atoms; red stars: experimental NEXAFS results.

structures and peaks at similar positions (see Fig. 3) . However, the agreement concerning the relative intensities of the peaks is not satisfactory: the GW DOS shows a steep rise above the vacuum level due to the presence of free electron states which instead do not contribute to the NEXAFS. As the character of the free electron states is completely different from the ones that we expect to give rise to the NEXAFS, we look at how many body effects are acting on the different states. In Fig. 4 we show the GW corrections and the expectation value of the exchange term $<\Sigma_x>$ as a function of KS energies. It can be seen that most of the GW corrections for the unoccupied states range between 0 and 1 eV, however there are a bunch of states with larger corrections. When we look at the values of $<\Sigma_x>$ the different character of these states becomes even more evident.

Since the magnitude of $<\Sigma_x>$ is linked to the degree of localization over the occupied states of the single-particle-state wavefunctions, it may provide a preliminary criterion to select the single particle states that contribute mostly to the experimental peaks present in the NEXAFS spectra, where the probed empty states must have a finite oscillator strength with the core-hole.

The set of empty states with $|\langle\Sigma_x\rangle| < 3.5$ eV is clearly isolated from the rest. By taking into account only the empty states that fulfill this condition (i.e. that lay below the dashed line in the bottom panel of Fig. 1), we obtain the DOS plotted in red in Fig. 5: the experimental peaks structure is still nicely reproduced with only 9 of the 145 empty states used in the full calculation, and the agreement concerning their relative intensity is improved. It is interesting to notice that similar results are obtaining projecting the total DOS onto the macrocycle carbon and nitrogen atoms orbitals (blue-dashed line in Fig.

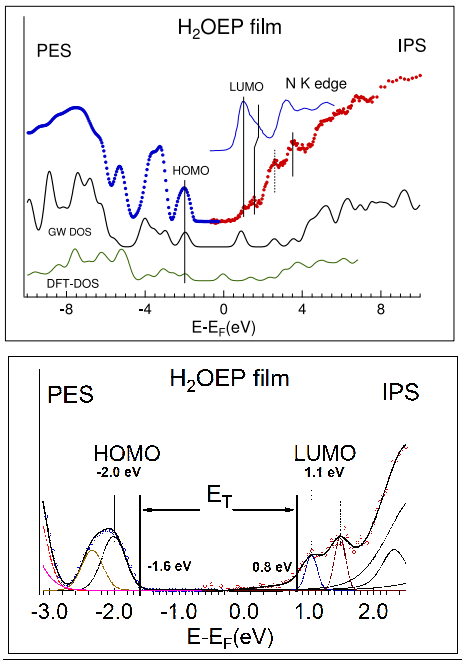

Figure 6 Top: Combined PES and IPS data (blue and red dots respectively) of the H_2OEP film together with the computed DOS (GW results: green line DFT results: orange line) and NEXAFS. Bottom: Frontier orbitals region of the combined PES and IPS spectra (open circles) of the H2OEP film. The lines are their fits and the relevant components. E_T indicates the transport gap

5).

Thin film phase Concerning the effect of crystal packing on the electronic properties of molecules, a decrease of the band gap was reported in corannulene-based materials[36], in crystalline rubrene[37], benzene, pentacene, C_{60}, and PTCDA[38–40]. Such changes in the electronic properties of the film with respect to the molecular phase might be caused by a geometry distortion within each molecule and/or an enhancement of the electronic screening. Interestingly, DFT in the standard KS approach was not able to capture this effect and it was compulsory to go beyond this level of description either by using hybrid functionals[38] or by employing MBPT[39,40].

Fig. 6 shows the combined experimental PES-IPS data of the H_2OEP thin film, the film phase N K edge NEXAFS, and the GW and DFT DOS computed for the triclinic structure. For clarity, the NEXAFS are plotted by aligning the LUMO peak to the first structure of the IPS, and the theoretical DOS are plotted by aligning the HOMO level with the experimental one.

The film transport gap E_T value of 2.4 +/- 0.2 eV, has been determined by the energy difference between the VB and CB onsets[8], as found by the least mean square fitting procedure of the experimental spectra. The lower panel of the figure

Table 2 Computed HOMO-1, HOMO, LUMO, LUMO+1 energy levels for the H_2OEP molecule in the triclinic phase. The absolute value of the energies is obtained by aligning the HOMO with experimental value.

Triclinic phase	HOMO-1 (eV)	HOMO (eV)	LUMO (eV)	LUMO+1 (eV)	GAP (eV)
DFT	-1.7	-1.6	0.2	0.3	1.8
GW	-1.7	-1.6	1.0	1.2	2.6
HF ($\Sigma_c = 0$)	-2.3	-1.6	4.8	4.9	6.4

Table 3 Electronic gap at the DFT, GW and HF level of the isolated molecule with distorted geometry.

	DFT	GW	HF ($\Sigma_c = 0$)
GAP (eV)	2.0	4.8	6.3

shows the frontier orbitals region of the combined PES and IPS measurements of the H_2OEP film. The dots correspond to the PES-IPS spectra. The lines are their fits and the relevant components. The vertical lines correspond to the VB (-1.6 eV) and CB (0.8 eV) onsets. The HOMO and LUMO peaks result at -2.0 eV and at 1.1 eV respectively. The the HOMO-HOMO-1 splitting is 0.35 eV, while LUMO and LUMO+1 splitting results 0.45 eV in IPS and 0.6 eV in N K edge NEXAFS (top panel).

In Tab. 2 we report, for the triclinic phase, the computed energy levels of the HOMO-1, HOMO, LUMO, and LUMO+1 states together with the values of the fundamental gap. Within the GW approach the value of the film electronic gap is 2.6 eV, in excellent agreement with the experimental finding of 2.4 ± 0.2 eV, especially when compared to the DFT value of 1.8 eV.

As in the case of other molecular crystals[36–40], the computed electronic gap of the film is significantly smaller than the isolated molecule gap (2.7 eV vs 4.7 eV). This effect is only found at the GW level: at the DFT level the gap is 1.8 eV, slightly smaller than the gap of the molecule in gas phase (2.0 eV).

In order to disentangle the effects of the geometry distortion from those of the increased electronic screening due to crystal packing, we performed a GW calculation for an isolated molecule whose geometry was kept fixed to the distorted one. The results are listed in Tab. 3: there is no shrinking of the electronic gap due to the geometry distortion; on the contrary, the GW electronic gap of the distorted molecule is slightly larger than in the equilibrium geometry (4.8 eV vs 4.7 eV).

The results of calculations where Σ_c was set equal to 0 are also shown in Tab. 1, Tab. 2, and Tab. 3. These calculations are equivalent to a non-self-consistent Hartree Fock calculation scheme where the wavefunctions are kept fixed to their KS values. Within this scheme, similarly to the case of DFT-

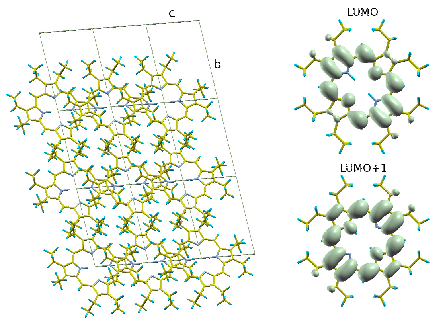

Figure 7 Left: stacking of the H_2OEP molecules within the triclinic structure. View from the (100) direction. Right: Isolated molecule LUMO and LUMO+1 electronic density isosurface at 2.5% of its maximum value.

KS results, the triclinic phase, the isolated molecule, and the isolated molecule in the distorted configuration have almost the same band gap. Since in this kind of calculations the electronic screening is not present, this further suggests that screening effects are at the origin of the difference of electronic gap of the two phases.

PES data show that in the film the HOMO-HOMO-1 orbitals energy separation is increased with respect to the gas phase. As well, IPS show that the LUMO and LUMO+1 levels, degenerate in gas phase, are split, indeed the broadening of the LUMO present in the N K edge NEXAFS could be related to such a splitting.

The origin of the LUMO and LUMO+1 degeneracy in the gas phase can be understood by looking at the electronic density isosurfaces of the two states, shown in the right part of Fig. 7. The LUMO and LUMO+1 degeneracy is linked to the 'square' symmetry of the macrocycle (indeed the macrocycle has a lower D2h symmetry due to the presence of the two H atoms). Taking into account the stacking of the molecules within the crystal (left panel of Fig. 7), it can be seen that the system becomes even less symmetric and the LUMO and LUMO+1 states are found split by ∼0.4 eV. In the calculations a splitting between these two levels is present as well, although it is of a smaller magnitude (0.2 eV). To further clarify this point we performed a calculation of the triclinic phase with an artificially distorted molecule. The molecule was distorted in the spirit of Ref.[46], namely, one of the two diagonals of the N-atoms square was stretched by 0.1 . All the atoms were rigidly shifted accordingly, so that finally only four C-C bond within the macrocycle were stretched. The resulting structure was higher in energy with respect to the most stable one of $\sim 6 \times 10^{-3}$ eV/atom. As a consequence of the square symmetry breaking, a larger LUMO and LUMO+1 splitting of ~ 0.3 eV was found already at the DFT level.

In Fig. 8 the total GW DOS of the isolated molecule and that of the film are presented together with their projections

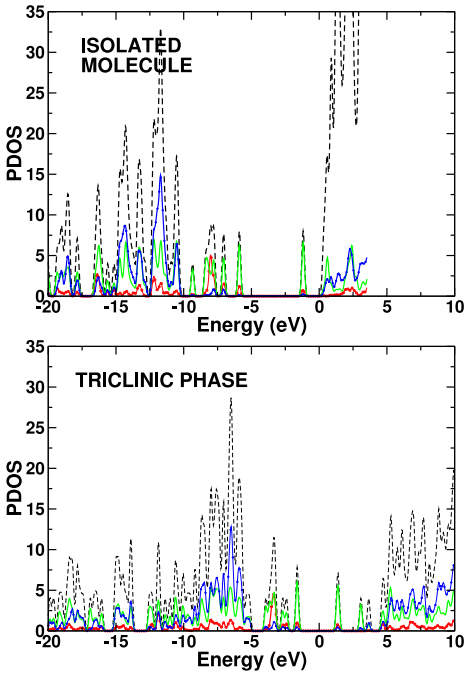

Figure 8 Projected DOS for the isolated molecule (top panel) and the triclinic phase (bottom panel). Dashed black lines: total DOS; red lines and points: N atoms contribution; green full lines: macrocycle C atoms contribution; blue lines and points: ethyl-groups C atoms contribution. In the isolated molecule case all energies are referred to the vacuum level, in the triclinic phase the HOMO is aligned to the experimental one.

onto the atomic orbitals of the nitrogen atoms, of the macrocycle carbon atoms, and of the ethyl-groups carbon atoms. The comparison of the projected DOS (PDOS) of the film and those of the isolated molecule shows that crystal packing does not alter qualitatively the distribution in energy of the electronic states belonging to the different parts of the molecule. At low energies, between -20 and -10 eV, the states have a mixed macrocycle and ethyl-group character, the latter becomes predominant between -10 and -5 eV, although the contribution from macrocycle atoms is not at all negligible also in this range of energies. Close to the gap, the electronic states belong, almost completely, to the macrocycle atoms. The total DOS of the isolated molecule rises promptly above the vacuum level, this rise is not present in the triclinic phase calculation and is addressable to the presence of free electron states whose density, moreover, depends on the size of the simulation cell. Apart from the magnitude of the HOMO-LUMO gap, and not taking into account the total DOS, the PDOS of the unoccupied states is again qualitatively similar to the one of the film: the LUMO is addressable mainly to the macrocycle atoms and the ethyl group contribution begins at higher energies.

4 Conclusions

In conclusion we carried out a combined experimental and theoretical investigation concerning the effects of crystal packing on the electronic properties of the H_2OEP molecule, focusing our attention on the unoccupied density of states and on the fundamental transport band gap. The unoccupied states of the film have been probed experimentally using IPS. This techniques yields direct information on the unoccupied energy levels in contrast to optical measurements where the joint-density of states is probed and many-body effects make the interpretation of spectra in terms of single particle transitions hardly possible[41].

On the theoretical level a quantitative description of the electronic properties of materials requires the inclusion of many-body effects going beyond DFT. We computed, for this purpose, GW correction to the DFT KS energy levels reaching a remarkable agreement with experiment.

In particular we found that, upon packing to form a molecular crystal, the H_2OEP molecule undergoes a sizable shrinking of the HOMO-LUMO gap. This effect is not due to the deformation of the geometry of the molecule, but to a more effective electronic screening in the 3D system. The computed electronic gap value of 2.6 eV is in excellent agreement with the experimental one of 2.4 eV. Square symmetry breaking, due to crystal packing and to possible distortions of the molecule, induces a splitting of the LUMO and LUMO+1 levels of ~ 0.4 eV. This effect is present also in the calculations although it is slightly underestimated.

Acknowledgments

This work is partially supported by the Italian Ministero dell'Istruzione, dell'Universitá e della Ricerca through the FIRB "Nanosolar" (contract No. RBAP11C58Y_003), the FIRB "SUPRACAR-BON" (contract No. RBFR10DAK6) and by the PRIN "GRAF" (contract No. 20105ZZTSE). The staff of Gas Phase Beamline (ELETTRA) is kindly acknowledged. The calculations have been performed at the CINECA HPC facility through the project ISC09, and at the ENEA CRESCO facility.

References

1 O. Loboda, Quantum-Chemical Studies on Porphyrins, Fullerenes and carbon Nanostructures, Carbon Nanostructures Vol XVIII, Springer-Verlag, Berlin Heidelberg (2013)
2 M. G. Walter, A. B. Rudine, and C. Wamser, J. Porphyrins and Phthalocyanines 14, 759 (2010)
3 M. Hambourger et al., Chem. Soc. Rev. 38, 25 (2009)
4 S. Mathew et al., Nat. Chem. 6, 242 (2014)
5 S. D. Pop, S. P. Kate. J. Rappich, and K. Hinrichs, Sol. En. Mat. Sol. Cells 127, 169 (2014)
6 M. Vasilopoulou et al., J. Mat. Chem. A 2, 182 (2014)
7 J. Cai et al., Soft Mat. 10, 2612 (2014)
8 D. R. T. Zahn, G. N. Gavrila, M. Gorgoi, Chem. Phys. 325, 99 (2006)
9 D. R. T. Zahn, G. N. Gavrila, and G. Salvan, Chem. Rev. 107, 1161-1232 (2007)
10 J. Xiao and P. A. Dowben, J. Phys.: Condens. Matter 21, 052001 (2009)
11 H. Yoshida, K. Tsutsumi, N. Sato, J. El. Spectr. Rel. Phen. 121, 83 (2001)
12 T. Schwieger, M. Knupfer, W. Gao, and A. Kahn, Appl. Phys. Lett. 83, 500 (2003)
13 S Krause, M B Casu, A Schll and E Umbach, New J. Phys. 10, 085001 (2008)
14 J. Wsten, S. Berger, K. Heimer, S. Lach, and Ch. Ziegler, J. Appl. Phys. 98, 013705 (2005)
15 C.I. Wu, Y. Hirose, H. Sirringhaus, A. Kahn Chem. Phys. Lett. 272 (1997)
16 J. H. Weaver, J. Phys. Chem. Solids 53, 1433 (1992)
17 M. , G. Koller, I. Kardinal, M. G. Ramsey, S. Stafstrm, and F. P. Netzer, J Chem. Phys. 110, 8060 (1999)
18 G. Rojas, X. Chen, C. Bravo, J-H Kim, J-S Kim, J. Xiao, P. A. Dowben, Y. Gao, X. Cheng Zeng, W. Choe, and A Enders, J. Phys. Chem. C, 114, 9408 (2010)
19 S. Rangan, S. Coh, R. A. Bartynski, K. P. Chitre, E. Galoppini, C. Jaye, and D. Fischer, J. Phys. Chem. C , 116, 2392 (2012)
20 G. Rojas, S. Simpson, X. Chen, D. A. Kunkel, J. Nitz, J. Xiao, P. A. Dowben, E. Zurekb, and A. Enders, Phys. Chem. Chem. Phys., 14, 4971 (2012)
21 S. Rangan, S. Katalinic, R. Thorpe, R. A. Bartynski, J. Rochford and E. Galoppini, J. Phys. Chem. C, 114, 1139 (2010)
22 N. E. Gruhn, D. L. Lichtenberger, H. Ogura, F. A. Walker, Inorg. Chem. 38, 4023 (1999)
23 G. Stenuit et al., Phys. Chem. Chem. Phys. 12, 10812 (2010)
24 J. W. Lauher and J. A. Ibers, J. Am. Chem. Soc. 95, 5148 (1973)
25 S. Dugar, R. Fu and N. S. Dalal, J. Phys. Chem. B 116, 9215-9222 (2012)
26 P. Borghetti et al., J. Chem. Phys. 138, 144702 (2013)
27 R. M. Dreizler and E. K. U. Gross, Density Functional Theory (Springer-Verlag, Heidelberg, 1990); R. O. Jones and O. Gunnarsson "The density functional formalism, its applications and prospects" Review of Modern Physics **61**, 689 (1989)

28 G. Onida, L. Reining, and A. Rubio, Rev. Mod. Phys. 74, 601 (2002)

29 M. M. Rieger, L. Steinbek, I. D. White, H. N. Rojas, and R. W. Godby, Comput. Phys. Commun., 117, 211 (1999)

30 H. N. Rojas, R. W. Godby, and R. J. Needs, Phys. Rev. Lett., 74, 1827,(1995)

31 A. Fleszar and W. Hanke. Phys. Rev. B, 56:10 228, (1997)

32 S. Lebgue, B. Arnaud, M. Alouani, and P. E. Bloehl. Phys. Rev. B, 67, 155208, (2003)

33 P. Giannozzi et al. J.Phys.: Condens. Matter, 21, 395502 (2002)

34 J. P. Perdew, K. Burke, and M. Ernzerhof , Phys. Rev. Lett. 77, 3865 (1996)

35 P. Umari, G. Stenuit, and S. Baroni, Phys. Rev. B 81, 115104 (2010)

36 L. Zoppi, L. Martin-Samos, K. K. Baldridge, J. Am. Chem. Soc. 133, 14002 (2011)

37 N. Sai, M. L. Tiago, J. R. Chelikowsky, F. A. Reboredo, Phys Rev. B 77, 161306(R) (2008)

38 S. Rafaely-Abramson, S. Sharifzadeh, M. Jain, R. Baer, J. B. Neaton, and L. Kronik Phys Rev. B 88, 081204(R) (2013)

39 J. B. Neaton, M. S. Hybertsen, S.G. Louie, Phys. Rev. Lett. 97, 216405 (2006)

40 S. Sharifzadeh, A. Biller, L. Kronik, and J.B. Neaton, Phys. Rev. B 85, 125307 (2012)

41 A. Ruini, M. J. Caldas, G. Bussi, and E. Molinari, Phys. Rev. Lett. 88, 206403 (2002)

42 Pure and Appl. Chem., 59, 779 (1987)

43 C. A. Hunter abd J. K. M. Sanders, J. Am. Chem. Soc. 112, 5525 (1990)

44 D. L. Cullen and E. F. Meyer Jr, J. Am. Chem. Soc. 96, 2095 (1974)

45 G. Di Santo, S. Blankenburg, C. Castellarin-Cudia, M.Fanetti, P.Borghetti, L.Sangaletti, L.Floreano, A. Verdini, E. Magnano, F. Bondino, C. A. Pignedoli, M-T. Nguyen, R. Gaspari, D. Passerone, A. Goldoni , Chem. A Eur. J. 17, 14354 (2011)

46 C.O. Fernandez, M. Kogan, A. Valasinas, and B. Frydman, J. Org. Chem. 63, 4829 (1998)